


RESEARCH ARTICLE



High throughput screening assay for the identification of ATF4 and TFEB activating compounds

Daniel J. Pfau and Ruslana Bryk 

Department of Microbiology and Immunology, Weill Cornell Medicine, New York, NY, USA


ABSTRACT

Macrophages act to defend against infection but can fail to completely prevent bacterial replication and dissemination in an immunocompetent host. Recent studies have shown that activation of a host transcription factor, TFEB, a regulator of lysosomal biogenesis, could restrict intramacrophage replication of the human pathogen *Mycobacterium tuberculosis*, and synergise with sub-optimal levels of the antibiotic rifampin to reduce bacterial loads. Currently available small molecule TFEB activators lack selectivity and potency but could be potentially useful in a variety of pathological conditions with suboptimal lysosomal activity. TFEB nuclear translocation and activation depend on its phosphorylation status, which is controlled by multiple cellular pathways. We devised a whole cell, high throughput screening assay to identify small molecules that activate TFEB by establishing a stably transfected HEK293T reporter cell line for ATF4, a basic leucine zipper transcription factor induced by stress response and activated in parallel to TFEB. We optimised its use *in vitro* using compounds that target endoplasmic reticulum stress and intracellular calcium signalling. We report results from screening the commercially available LOPAC library and the Selleck Chemicals library modified to include only FDA-approved drugs and clinical research compounds. We identified 21 compounds across six clinical use categories that activate ATF4 and confirmed that two proteasome inhibitors promote TFEB activation. The results of this study provide an assay that could be used to screen for small molecules that activate ATF4 and TFEB and a potential list of compounds identified as activators of the ATF4 transcription factor in response to cellular stress.

ARTICLE HISTORY Received 10 July 2024; Revised 16 January 2025; Accepted 16 January 2025

KEYWORDS Host-directed therapy; macrophage; mycobacteria; stress response; tuberculosis

CONTACT Ruslana Bryk  rub2001@med.cornell.edu Department of Microbiology and Immunology, Weill Cornell Medicine, Weill Cornell Medicine, 413 East 69 Street, New York, NY 10021, USA

 Supplemental data for this article can be accessed online at <https://doi.org/10.1080/27694127.2025.2473765>

© 2025 The Author(s). Published by Informa UK Limited, trading as Taylor & Francis Group.

This is an Open Access article distributed under the terms of the Creative Commons Attribution-NonCommercial License (<http://creativecommons.org/licenses/by-nc/4.0/>), which permits unrestricted non-commercial use, distribution, and reproduction in any medium, provided the original work is properly cited. The terms on which this article has been published allow the posting of the Accepted Manuscript in a repository by the author(s) or with their consent.

Introduction

Tuberculosis is the global leader in infectious disease mortality. Current treatments are effective, but lengthy, toxic and lead to the development of multi-drug resistant strains, for which treatment options are limited. Host-directed therapy (HDT) aims to enhance treatment efficacy by targeting host pathways involved in pathogen control and clearance and contribute to reducing tissue inflammation and lung pathology to improve patient outcomes [1–3]. *Mycobacterium tuberculosis* (Mtb) exploits lysosome-poor monocyte-derived lung cells for persistence during chronic infection [4] and subverts effective immune responses [5]. Some of the mechanisms used by Mtb to escape immunity within the macrophage include inhibition of phagosomal maturation [6–8] and phagolysosomal fusion [9], modulation of cytokine production [10,11] and manipulation of gene expression by non-coding RNAs [12,13]. Therapeutic interventions directed at improving the lysosomal function of host cells may contribute to better restriction of bacterial growth and augment conventional antibiotic therapy.

Our previous studies identified TFEB as a potential target for HDT during Mtb infection and reported that the compound 2062 [14], which shows no direct antimycobacterial activity, promoted activation of TFEB in macrophages and synergised with suboptimal rifampin to further reduce Mtb colony forming units (CFU) in macrophages and in mice, as well as to reduce lung pathology in infected mice [14]. C-Abl kinase inhibitors, imatinib and nilotinib, were reported to promote TFEB activation and lysosomal activation and to reduce bacterial loads in Mtb infected macrophages and mice [4]. Recent studies have also demonstrated that bedaquiline, an antibiotic currently used for the treatment of drug-resistant Mtb, activates host TFEB, which may contribute to its efficacy *in vivo* [15]. TFEB activation during bacterial infection was also reported to promote the production of itaconate, which has antimicrobial properties and could contribute to bacterial clearance [16]. Collectively, these data suggest that TFEB activation could be beneficial to the host infected with Mtb and may improve treatment outcomes if used as an adjunct HDT along with TB antibiotics.

TFEB activation is controlled by its phosphorylation on multiple serine residues [17–21]. TFEB dephosphorylation by the Ca^{2+} /calmodulin-dependent phosphatase calcineurin or PP2A or a reduction in phosphorylation through inhibition of upstream kinases (mTOR, ERK, Akt, GSK3b) promotes TFEB nuclear translocation and activation. Since TFEB activating compounds do not act on the TFEB protein itself, but instead target multiple signalling pathways upstream of TFEB, they usually lack specificity. Recent interest in TFEB activators and their utility resulted in a few reports [22–24] identifying a limited number of small molecules able to activate TFEB, including natural products such as curcumin analogue C1 [25], celastrol [26],

resveratrol [27], digoxin [22] and ikarugamycin [22]. However, those molecules are not selective, do not robustly activate TFEB, and are reported to have many other competing activities.

Identification of new TFEB activators often relies on microscopic evaluation of TFEB nuclear translocation, which is limited by its poor robustness, low throughput, and heterogeneity in cellular responses. Therefore, our goal was to develop a new screening assay in a whole cell high throughput format to enable and streamline the identification of small molecule activators of TFEB. We decided not to follow TFEB nuclear translocation itself using high content imaging as a primary screening platform but to develop a reporter gene readout to improve screen robustness and increase throughput. We took advantage of the observation that compound 2062, a TFEB small molecule activator [14], had an early transcriptional signature of a cellular stress response and led to prominent upregulation of the ER stress response genes, including the activating transcription factor 4 (ATF4). ATF4 expression is regulated by PERK and eIF2alpha phosphorylation, one of the pathways that also activates TFEB. TFEB activation was also reported to promote ATF4 expression [28], demonstrating the interdependence of both signalling pathways.

Here, we report the development of a stable ATF4 transcription reporter HEK293T cell line and optimisation of the luminescence read-out using the SERCA inhibitor thapsigargin and the endoplasmic reticulum (ER) stress inducer tunicamycin. We then screened two libraries, totalling more than 3000 compounds, including a library of clinical research compounds comprised of drugs with suitable human use profiles. From the top 48 compounds, 21 reproducibly activated ATF4 transcription signal in our transfected cell line at a concentration of 4 μ M after 24 hours. We used secondary microscopy evaluation of TFEB nuclear translocation on the hit compounds identified in the screen to select the ones that also activated TFEB. The secondary screen confirmed that two of the compounds, carfilzomib and bortezomib, strongly activate TFEB in mouse bone marrow derived macrophages (BMDM). Collectively, our studies provide a method for screening small molecules that activate ATF4 transcription and TFEB nuclear translocation in response to stress and provide a list of compounds that may represent TFEB activating compounds. These results may further justify an expanded screening effort for compounds that activate TFEB.

Results

We hypothesised that ATF4 transcription could serve as reporter to identify compounds that activate TFEB downstream of cellular stress and also avoid identifying compounds downstream of mTOR inhibition, which could immunosuppress the host. We confirmed that in response to TFEB activating

conditions, either starvation or ER stress, we can observe TFEB dephosphorylation and ATF4 upregulation at the protein level (Figure 1). Western blots of Raw 264.7 cells cultured in either HBSS or cDMEM supplemented with 1 μ g/mL tunicamycin for 7 hours demonstrated a reduction in the cytosolic levels of TFEB most likely reflecting dephosphorylation and its nuclear translocation. These samples also showed significant upregulation of ATF4 protein expression (Figure 1) demonstrating that both ATF4 and TFEB are upregulated/activated in a mouse macrophage cell line in response to these stresses.

To develop a high throughput screen, we produced a stably transfected HEK293T cell line using a commercially available Promega vector pNL (NlucP/ATF4-RE/Hygro). This vector encodes a NanoLuc luciferase, a genetically

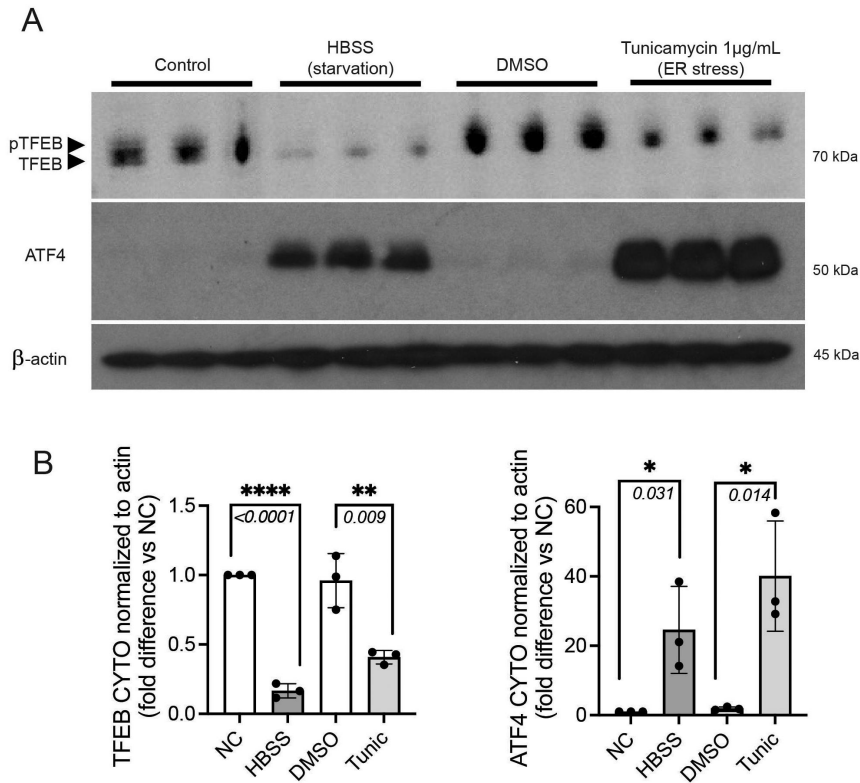


Figure 1. TFEB and ATF4 are activated in parallel in Raw 264.7 cells during starvation and ER stress. (A) Triplicate samples were prepared for all conditions, cells were collected after 7 h of exposure to select conditions or agents, lysed in RIPA buffer supplemented with protease inhibitors, and soluble lysates fractionated on SDS-PAGE and immunoblotted by WB. (B) TFEB (left) and ATF4 (right) levels in panel A were quantified in Fiji (ImageJ), normalised to actin loading in each lane, and compared to control sample (NC) designated as “1”. Data shown are means \pm SD of triplicate values. Statistical analysis was carried out by the Student’s t test, P values are shown in the comparison brackets. NC, control; Tunic, tunicamycin.

optimised luciferase to produce the strongest luminescent signal among the currently available luciferase reporters, under the control of the ATF4 response element. We selected the HEK293T cell line for the development of the reporter cell line for the ease of its transfection and manipulation and optimised transfection conditions with the pNL vector by testing different transfection reagents (Lipofectamine 3000 and Lipofectamine LTX), times of transfection, reagent volumes, and amounts of DNA transfected (Supplemental Table 1). Luminescence after each transfection was measured, normalised to untreated cells, and tested for the signal response window after 6.5 – 7.5 hours treatment with either 1 μ M thapsigargin or 3 μ M 2062 [14] (Supplemental Figure 1). We selected transfection conditions (#6, Supplemental Table 1) that produced the greatest percent increase in signal (150–200%) relative to controls and selected transfected populations with either 150 μ g/mL or 300 μ g/mL hygromycin. Once cells had grown to sufficient density for passaging and testing, they were tested for their ability to luminesce when stimulated with 1 μ M thapsigargin. During treatment, cells selected in 300 μ g/mL hygromycin displayed a greater response to stimulation, and were used in all further experiments. At this concentration of hygromycin, the presence of the selection agent during drug treatment or assay visualisation did not impact ATF4 transcription at baseline or after stimulation (Supplemental Figure 2).

We characterised the cell line by measuring ATF4 transcription response over time to select compounds including the SERCA inhibitor thapsigargin, the ER stress inducer tunicamycin, the mTOR inhibitor torin 1 and the experimental compound 2062, as well as the antitubercular drugs bedaquiline, rifampin, and isoniazid. Of these compounds, thapsigargin and tunicamycin, both ER stress inducers, produced the greatest signal within 28 hours (Figure 2), as expected. Relative to controls, 2062 also produced increased luminescence within 28 hours.

Next, we determined the concentration-response of HEK293T pNL(NlucP/ATF4-RE/Hygro) to thapsigargin and tunicamycin treatment over time (Figure 3A–B). Duration and intensity of the luminescent signal were dependent on compound concentration. Increasing concentrations of tunicamycin produced the greatest signal, while the opposite effect was observed for thapsigargin. The effect of thapsigargin on reporter luminescence was not associated with toxicity, as microscopic evaluation confirmed that the monolayers were not affected by treatment. Both thapsigargin and tunicamycin produced a significant increase in signal by 26.5 hours at both the lowest and highest doses tested. Next, we optimised the cell density for a 384 well plate and HTS format by measuring luminescence after 24 hours of treatment with thapsigargin (Figure 3C). We optimised the cell seeding to 3×10^4 cells per well, which did not result in overgrowth after 24 hours of culture in the base medium (cDMEM with 300 μ g/mL hygromycin), and produced the maximum amount of signal (Figure 3C).

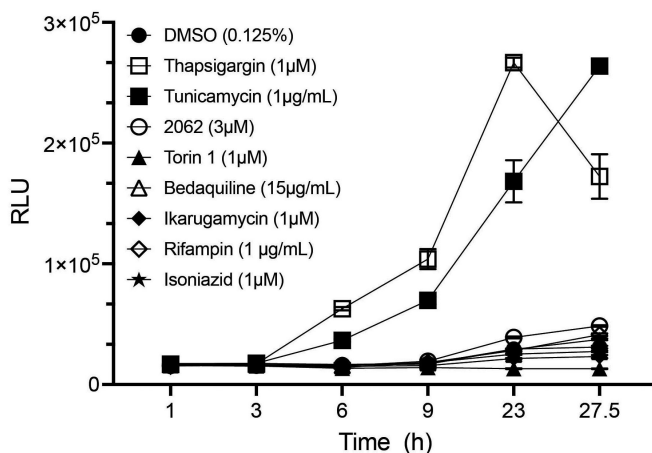


Figure 2. HEK293T pNL(NlucP/ATF4-RE/Hygro) cells respond to ER stress reagents with increase in ATF4 reporter luminescence. Data is mean \pm SD of triplicate wells from a representative experiment repeated at least twice with similar results.

Assay reproducibility was assessed by using the commercially available LOPAC library at the Rockefeller University Fisher Drug Discovery Resource Center (DDRC). The LOPAC library was dispensed into a base culture medium containing 300 μ g/mL hygromycin in 384 well plates, and cells were seeded at 3×10^4 cells per well. The final concentration of compounds in each well was 4 μ M, a concentration previously determined to be sufficient to induce significant signal and minimal cytotoxicity observable by microscopy with both thapsigargin and tunicamycin. DMSO and 1 μ M thapsigargin were included in columns 23 and 24, respectively, as negative and positive controls for all plates tested. Luminescence was measured with the nano-Glo Luciferase Assay after 24 h of exposure to test compounds. Data were uploaded to the Collaborative Drug Discovery website and matched with heat maps of signal produced per well (Figure 4A). This assay was then repeated 2 days later. Values from the two independent experiments were plotted against each other, including positive and negative control wells from all plates, and are represented in a scatter plot fitted with a linear best fit line (Figure 4B). The calculated R^2 was 0.933. The top hits from the LOPAC library included calcimycin, a calcium ionophore as well as thapsigargin, the positive control used for optimisation of the assay, and diphenyleneiodonium chloride, an NADPH oxidase inhibitor and a generator of oxidative stress.

Next, we screened a modified Selleck Chemicals library of 1800 compounds at the Fisher DDRC, which included FDA-approved drugs and clinical research compounds. Compounds that produced activation above 50% of the signal increase observed with the positive control were selected for testing in confirmation and concentration-response assays. The top 35 hits

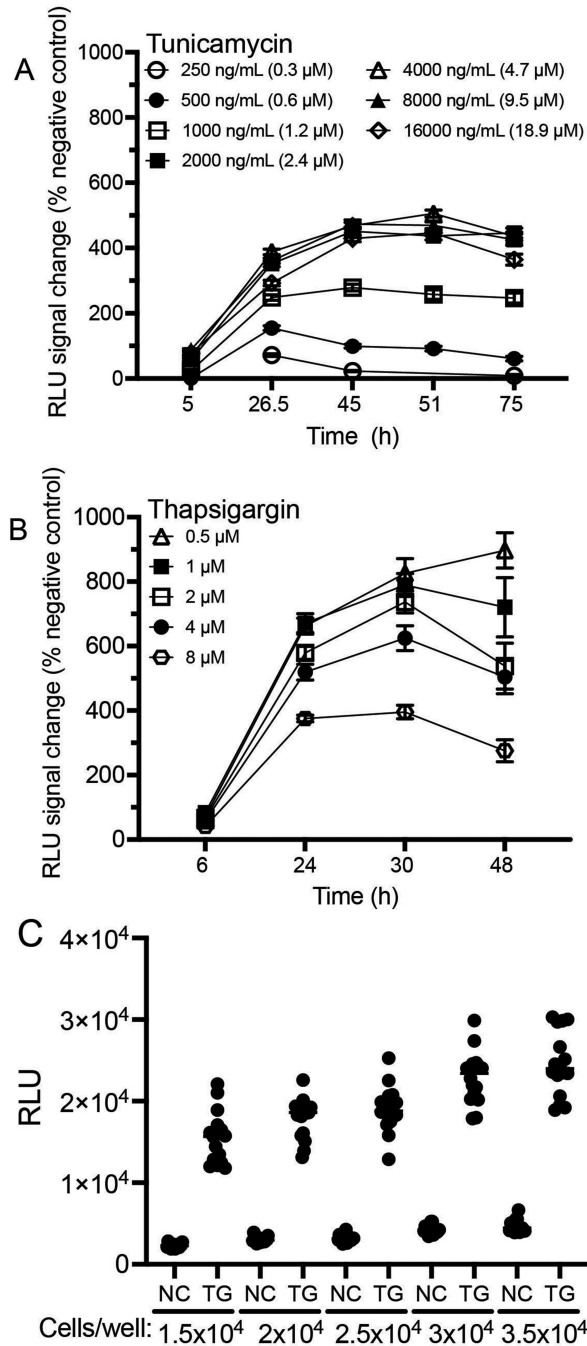


Figure 3. HEK293T ATF4 reporter luciferase assay optimisation and characterisation. Stably transfected HEK293T cells were treated with either thapsigargin or tunicamycin at indicated concentrations. Equal volume of the nano-Glo reagent (Promega) was added at indicated times and luminescence recorded. Dose response curves for the luminescent signal generated in response to treatment with tunicamycin (A) or thapsigargin (B).

are listed side-by-side in [Table 1](#) including the hit compounds from the original screen, the cherry-picked hits from the confirmation plate, and the results from the 4 μM concentration point within each dose response curve. From those listed, 21 drugs were consistently identified across all assays and represented six clinical categories of drugs (Supplemental Figure 3).

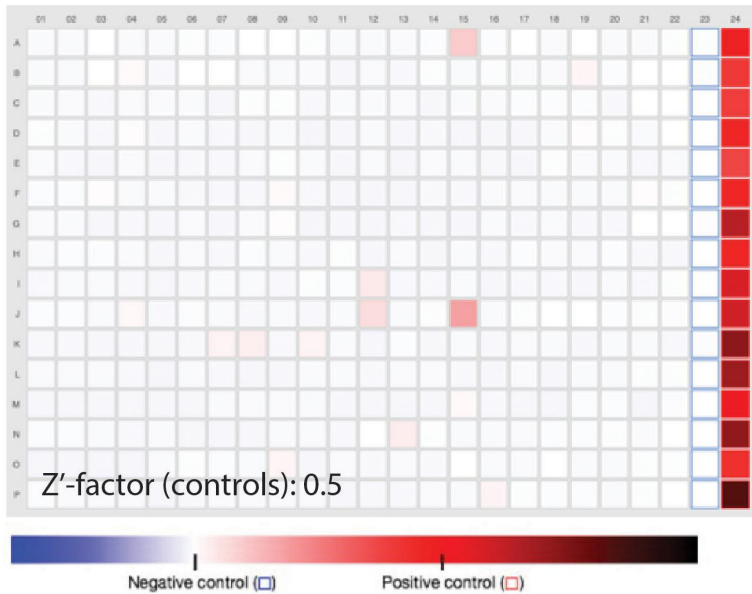
Dose response curves were assessed by luciferase assay after 24 hours of treatment, starting at a maximum dose of 8 μM and including 11 twofold serial dilutions and the EC_{50} values were calculated. The top five most potent activators of ATF4 transcription were artemisinin and four of its derivatives (Supplemental Figure 4). These results are consistent with a report that artesunate is capable of activating stress responses and ATF4 expression in cancer cells [29]. Accordingly, our studies demonstrate activation of ATF4 in our stably transfected cell line with artemisinin and its derivatives at sub-micromolar range, and show calculated EC_{50} values all less than 0.05 μM . The anticancer drug doxorubicin and the antidiarrheal nifuroxazide also exhibit EC_{50} values below 1 μM .

To determine if the compounds identified in the screen activate TFEB, we used WB and immunocytochemistry to directly measure TFEB translocation in mouse BMDMs in response to treatment with test compounds. BMDM treated with bortezomib or carfilzomib robustly activated both, ATF4 and TFEB, as detected by WB with anti-TFEB and anti-ATF4 immunoblotting of nuclear fractions of cells treated with 4 μM of either compound or an increasing dose of bortezomib ([Figure 5](#)). Bortezomib at a concentration of 10 nM was able to strongly activate TFEB nuclear translocation within 2 h of exposure. Artemisinin was also able to activate the TFEB as detected by the WB ([Figure 5](#)).

Accordingly, immunocytochemistry demonstrated a significant increase in intranuclear mean fluorescence intensity relative to untreated controls, indicating TFEB translocation, for thapsigargin and torin 1 ([Figure 6A](#)), as well as proteasome inhibitors bortezomib and carfilzomib ([Figure 6B](#)). Given that proteasome inhibitors bortezomib and carfilzomib consistently activated TFEB and the response was observed early (2 h of exposure) and at low nM concentrations, we thought to test if proteasome inhibitors developed against Mtb [30,31] will demonstrate any effect on host cells by activating TFEB. We selected two different Mtb proteasome inhibitors with comparable

(C) Cells were seeded at the indicated densities and treated with 1 μM thapsigargin for 24 hours before measuring luminescence. Results are expressed as percent increase in signal relative to negative controls (no treatment) in (A), (B) using mean \pm SD of triplicate wells or as Relative Luminescent Units (RLUs) with individual values per each well in (C). Each experiment was repeated at least three times with similar results.

A



B

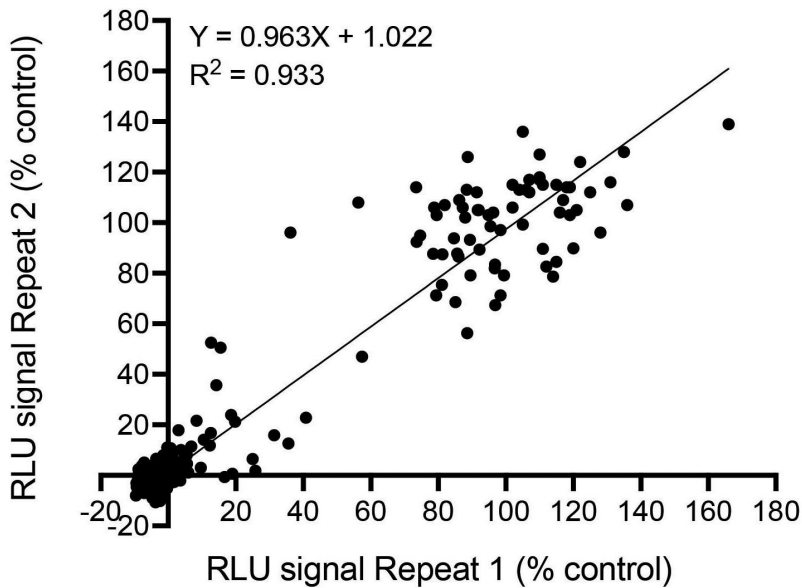


Figure 4. LOPAC compound library screen using HEK293T pNL(NlucP/ATF4-RE/Hygro) cell line. Luminescence was measured with nano-Glo reagent after exposure to 4 μ M test compound for 24 hours at a cell density of 3×10^4 cells/well. (A) Representative heat map from a screen, Z'-factor for the plate is indicated. (B) Scatter plot of percent activation from separate LOPAC assays on separate days. Plot includes positive and negative control wells from all plates screened on each day. Included within the plot are the best fit line equation and R^2 values calculated in Prism GraphPad 10. Top hits identified in the screen included calcimycin, thapsigargin, azacytidine, dequalinium, tryphostin A9, nalbuphine, tryphostin AG 879, brefeldin A, AC-93253 iodide, and diphenyleneiodonium.

Table 1. Modified Selleck Chemicals library screen and follow-up luciferase assay results. The top 35 HTS hits are listed in descending order by % activation relative to the positive control for three separate assays side by side – screen, confirmation plate, and the 4 μ M concentration from the EC₅₀ assay. The common 21 compounds identified in the top 35 in all three assays are bolded.

Screen (4 μM)			Confirmation plate (4 μM)		4 μM from EC50 curve	
Drug name	Rockefeller ID	Drug name	Rockefeller ID	Drug name	Rockefeller ID	
Tirofiban	RU-0423089	Azacytidine	RU-0000555	Artemether	RU-0603322	
Nifuroxazide	RU-0024186	Cloxiquine	RU-0000080	Artemotil	RU-0603391	
Artemotil	RU-0603391	Nitrofurantoin	RU-0000209	Amsacrine	RU-0084027	
BGP-15	RU-0422977	COTI-2	RU-0603313	Nifuroxazide	RU-0024186	
Artemether	RU-0603322	Pentamidine Isethionate	RU-0000376	Carfilzomib	RU-0603278	
AT101	RU-0001105	Ritlecitinib	RU-0603516	Dihydroartemisinin	RU-0162021	
Artemisinin	RU-0083438	Furaltadone	RU-0083728	Artesunate	RU-0603318	
Puromycin	RU-0000464	Clotrimazole	RU-0000060	PF-04457845	RU-0603386	
Regorafenib	RU-0187357	Triethyl citrate	RU-0430425	Ascininib	RU-0603476	
COTI-2	RU-0603313	Nicardipine	RU-0000408	Bortezomib	RU-0279322	
Efmiconazole	RU-0430527	Parthenolide	RU-0603356	Puromycin	RU-0000464	
Pentamidine Isethionate	RU-0000376	Nifuroxazide	RU-0024186	(-)Arctigenin	RU-0187041	
Cloxiquine	RU-0000080	Artemisinin	RU-0083438	Azacytidine	RU-0000555	
Carfilzomib	RU-0603278	Regorafenib	RU-0187357	Furaltadone	RU-0083728	
Chlorhexidine	RU-0000038	Doxorubicin	RU-0162123	COTI-2	RU-0603313	
Furaltadone	RU-0083728	(-)Arctigenin	RU-0187041	Nitrofurantoin	RU-0000209	
Clotrimazole	RU-0000060	AT101	RU-0001105	Ledipasvir	RU-0603477	
(-)Arctigenin	RU-0187041	Ledipasvir	RU-0603477	Artemisinin	RU-0083438	
Azacytidine	RU-0000555	Carfilzomib	RU-0603278	Doxorubicin	RU-0162123	
Ritlecitinib	RU-0603516	Puromycin	RU-0000464	Regorafenib	RU-0187357	
Artesunate	RU-0603318	Tasimetleone	RU-0430376	Pentamidine Isethionate	RU-0000376	
Amsacrine	RU-0084027	Dihydroartemisinin	RU-0162021	JNJ-42165279	RU-0603384	
Frovatriptan Succinate	RU-0430365	Erlotinib	RU-0187358	Parthenolide	RU-0603356	
Resveratrol	RU-0001031	Resveratrol	RU-0001031	Amonafide	RU-0279423	
Ascininib	RU-0603476	Frovatriptan Succinate	RU-0430365	Cloxiquine	RU-0000080	
Dihydroartemisinin	RU-0162021	Bortezomib	RU-0279322	Sanguinarine	RU-0000871	

(Continued)

Table 1. (Continued).

Screen (4 μ M)		Confirmation plate (4 μ M)		4 μ M from ECso curve	
Drug name	Rockefeller ID	Drug name	Rockefeller ID	Drug name	Rockefeller ID
Oleanolic Acid	RU-0279596	Disulfiram	RU-0000115	Dehydrocostus Lactone	RU-0423099
Acotiamide	RU-0430681	Asciminib	RU-0603476	AT101	RU-0001105
Bortezomib	RU-0279322	Dehydrocostus Lactone	RU-0423099	Ritlectinib	RU-0603516
Lanifibranor	RU-0430678	549076	RU-0422735	Oleanolic Acid	RU-0279596
Leonurine	RU-0430410	Tirofiban	RU-0423089	Nicardipine	RU-0000408
Parthenolide	RU-0603356	Sanguinarine	RU-0000871	Erlotinib	RU-0187358
Disulfiram	RU-0000115	Tenofovir Disoproxil	RU-0430780	Resveratrol	RU-0001031
PF-04457845	RU-0603386	Lanifibranor	RU-0430678	Clotrimazole	RU-0000060
Tenofovir Disoproxil	RU-0430780	Amsacrine	RU-0084027	Disulfiram	RU-0000115

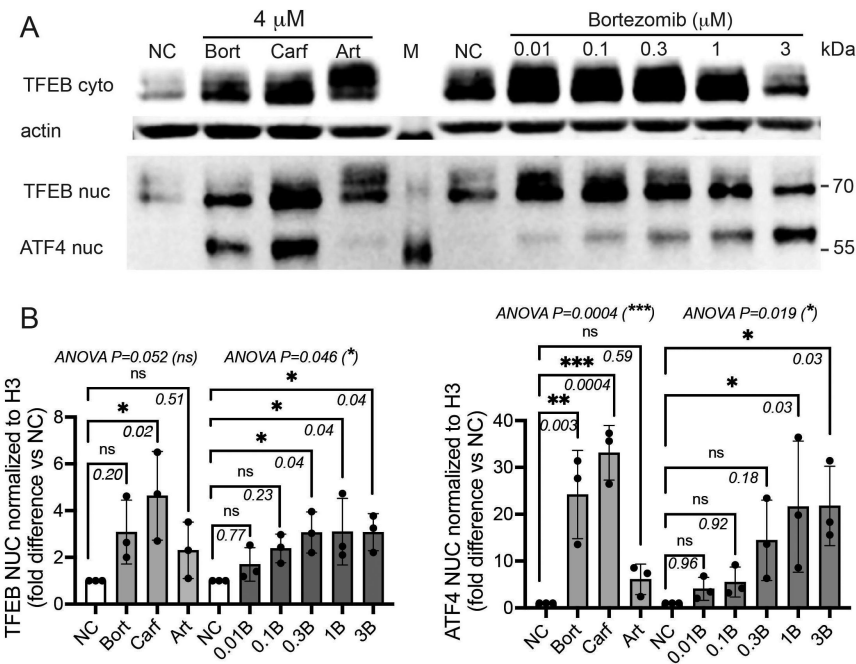


Figure 5. Proteasome inhibitors, bortezomib and carfilzomib, promote TFEB and ATF4 activation in a dose-dependent manner in BMDM. (A) Cells were exposed to indicated concentrations of inhibitors for 2 h and cell extracts were separated into cytosolic (top) and nuclear (bottom) fractions, fractionated on 10% SDS-PAGE and WB with anti-TFEB (1:2500), anti-actin (1:5000), and anti-ATF4 (1:1000). NC, vehicle control; M, MW marker; Bort, bortezomib; Carf, carfilzomib; Art, artemisinin. Shown is a representative blot from three independent repeats. (B) Nuclear TFEB (left) and ATF4 (right) levels in panel A were quantified in Fiji (ImageJ), normalised to histone H3 loading in each lane, and compared to control sample (NC) designated as “1”. Data shown are means \pm SD of three independent experiments using primary cells from three different mice. Statistical analysis was carried out by ANOVA, adjusted P values for multiple comparisons were obtained from the Dunnett’s test and are shown in the comparison brackets. Numbers at the X-axis correspond to the μ M bortezomib concentrations (0.01B, 0.1B, 0.3B, 1B, 3B); ns, not significant at the confidence level of 95%.

potency against the Mtb proteasome but variable, high (>13,000-fold) and low (11-fold) selectivity for the Mtb proteasome over human constitutive and immunoproteasome and observed that the highly selective proteasome inhibitor **6** [31], which does not inhibit human proteasome in vitro, did not activate TFEB in BMDM while the less selective inhibitor **11** [31], which inhibits human constitutive and immunoproteasome with submicromolar potency, promoted TFEB activation and nuclear translocation within 2 h of exposure as determined by TFEB WB in nuclear extracts of BMDM exposed to 1 μ M inhibitors for 2 h (Figure 7). These findings are consistent with our prior

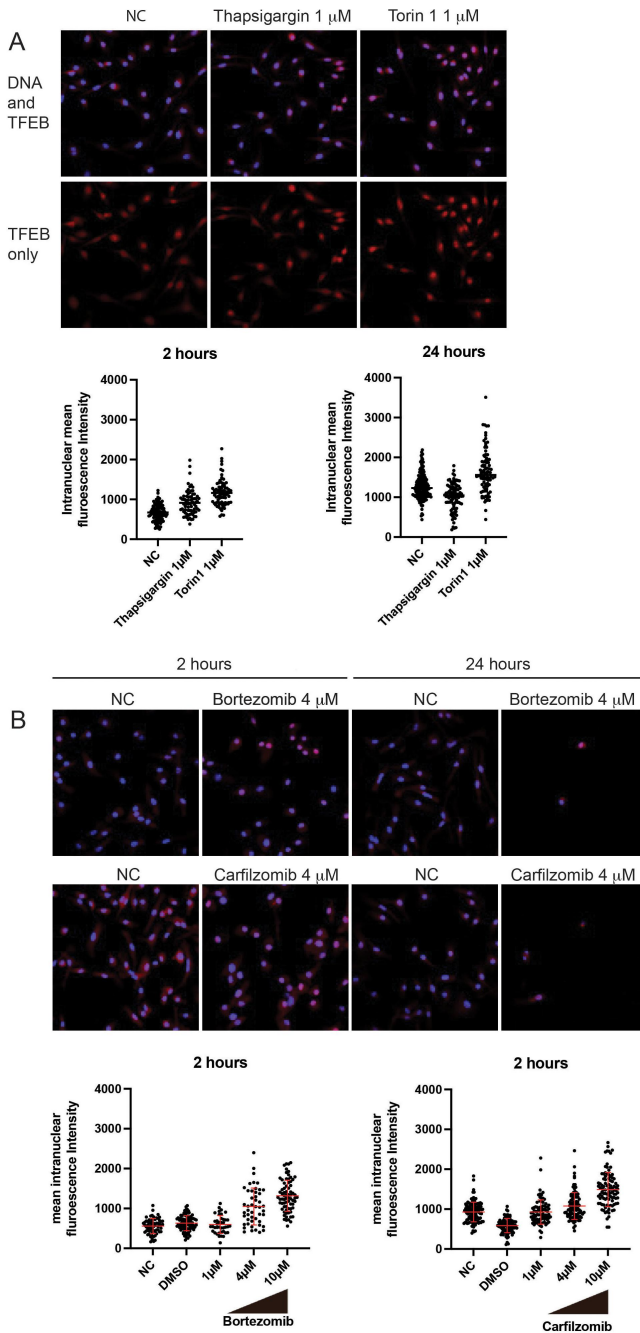


Figure 6. Proteasome inhibitors carfilzomib and bortezomib activate TFEB in mouse BMDM. BMDM were treated for the indicated times before fixation, permeabilization and staining. All images shown are 40x magnification. (A) Control compounds, thapsigargin and the mTOR inhibitor torin1, promote TFEB nuclear translocation as measured by immunocytochemistry. Images shown are 2 hours after treatment. Intranuclear pixel intensity was measured and plotted. (B) Carfilzomib and bortezomib treatment promotes TFEB nuclear translocation in BMDM.

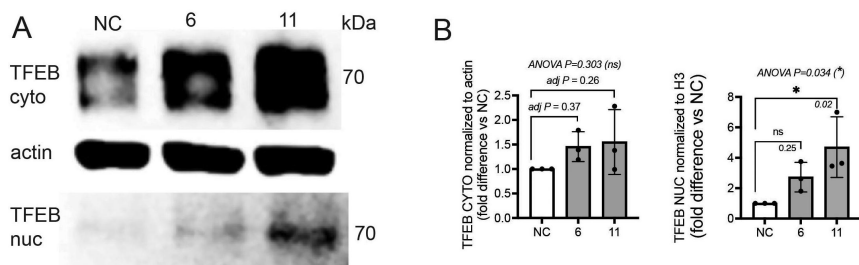


Figure 7. BMDM exposed to Mtb proteasome inhibitors activate host TFEB. (A) BMDM were treated with 1 μ M inhibitors for 2 h and cellular extracts were separated into the cytosolic (top) and nuclear (bottom) fractions and WB with anti-TFEB, and anti-actin. Shown is a representative blot from three independent repeats. Proteasome inhibitors **6** and **11** were previously published [31]. (B) TFEB cytoplasmic (left) and nuclear (right) levels in panel A were quantified in Fiji (ImageJ), normalised to actin (left) or histone H3 (right) loading in each lane, and compared to vehicle control (NC) designated as “1”. Data shown are means \pm SD of three independent experiments using primary cells from three different mice. Statistical analysis was carried out by ANOVA, adjusted P values for multiple comparisons were obtained from the Dunnett’s test and are shown in the comparison brackets.

observations that proteasome inhibitors promote TFEB activation and suggest that less selective Mtb proteasome inhibitors could act on both bacterial and host targets to improve Mtb control.

Finally, we tested if the TFEB-activating compounds identified in the screen were able to promote cellular activities such as autophagy, known to be associated with TFEB activation. Both bortezomib and carfilzomib, which identified as the most robust activators of TFEB, promoted autophagy as determined by the time-dependent increase in LC3-II in WB of cellular extracts prepared from BMDM exposed to bortezomib or carfilzomib for 6 h (Figure 8A). Increase in LC3-II upon exposure to bortezomib or carfilzomib was also accompanied by an increase in p62 (Figure 8A), a known autophagic substrate. While this increase in p62 in the presence of proteasome inhibitors is well documented and is associated with an improved autophagy [32,33] it could also indicate a block in the autophagic flux. Therefore, we further explored the effect of two of our hit compounds, bortezomib and artemisinin, on the autophagic flux in BMDM in the presence of bafilomycin A1, a V-ATPase inhibitor that prevents autophagosome-lysosome fusion and is used to quantify cellular autophagic flux [34]. We exposed the cells to bafilomycin A1 (100 nM), bortezomib (3 μ M), or artemisinin (3 μ M) alone and for our two test agents also in combination with bafilomycin A1 and compared the levels of LC3-II accumulation by bortezomib and artemisinin in the absence and presence of bafilomycin A1 by WB (Figure 8B) and ImageJ analysis (Figure 8C) from four independent experiments that used different

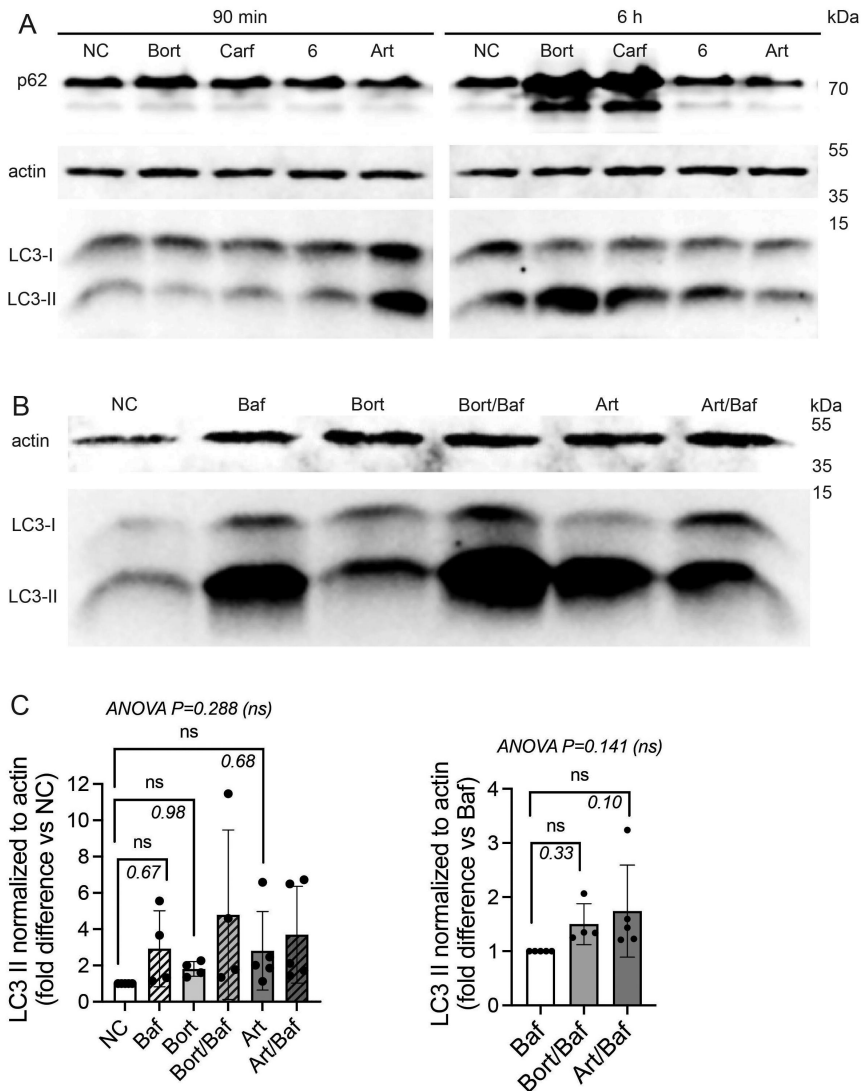


Figure 8. BMDM exposed to TFEB activating compounds promote autophagic flux. (A) BMDM were treated with indicated test compounds at 3 μ M for 90 min (left) or 6 h (right), soluble cellular extracts were separated on 15% SDS-PAGE and WB with anti-p62 (1:1000), anti-actin (1:2000), and anti-LC3 (1:1000). NC, vehicle control; Bort, bortezomib; Carf, carfilzomib; **6**, proteasome inhibitor previously published [31]; Art, artemisinin. Shown is a representative blot from two independent repeats. (B) BMDM were exposed to 3 μ M Bort, 3 μ M Art, or 100 nM Bafilomycin A1 (Baf) alone or in combinations (Bort/Baf and Art/Baf) for 5 h, and soluble cellular extracts were separated on 15% SDS-PAGE and WB with anti-actin (1:2000), and anti-LC3 (1:1000). Shown is a representative blot from four independent repeats. (C) LC3-II levels were quantified in Fiji (ImageJ), normalised to actin and plotted in comparison to vehicle control (NC) (left) or Baf-treated samples (right). Data shown are means \pm SD of four independent experiments using primary cells from four different mice. Statistical analysis was carried out by ANOVA, adjusted P values for multiple comparisons were obtained from the Dunnett's test and are shown in the comparison brackets; ns, not significant at the confidence level of 95%.

mice for primary cell isolation. Our results demonstrate that both bortezomib and artemisinin improve autophagic flux (Figure 8C, right panel) albeit to a small degree, which could reflect the specific compound concentrations and treatment durations chosen for this experiment. We also observed significant variability between our experiments, which, most likely, reflects the variability in biological replicas using different mice to collect our experimental data. Nevertheless, we observed a consistent improvement in the autophagic flux of BMDM treated with bortezomib and artemisinin (Figure 8C).

Discussion

Macrophages act as a first line of defence against bacterial infection but can also serve as a significant bacterial reservoir within the host [4,35]. Mtb replication in a macrophage is controlled by the host's intracellular signalling, with interferon- γ -dependent effector pathways responsible for most of the restrictions imposed on Mtb growth. TFEB expression and activation represent one of the host's interferon- γ dependent mechanisms that contribute to Mtb control [14]. However, Mtb evolved to resist and evade immune recognition by arresting phagosomal maturation and acidification and adapted to exploit lysosome-poor monocyte-derived lung cells to persist during chronic infection [4]. We hypothesised that HDTs that activate TFEB, a transcription factor regulating genes involved in lysosomal biogenesis and maturation may act to improve specific host and organelle-level deficiencies exploited by intracellular pathogens for survival both in the acute and chronic phases of infection. To develop a screening method to identify such small molecules, we established a stably transfected, ATF4 transcription reporter cell line, characterised and optimised it for an HTS format and validated it by screening two small compound libraries.

The choice of ATF4 induction as a readout in our screening assay stemmed from a few observations: i) TFEB activating compound 2062 produced an early transcriptional signature of cellular stress response and led to prominent upregulation of ER stress response genes, including ATF4 [14]; ii) ATF4 and TFEB activation occur in parallel as ATF4 expression is regulated by PERK and eIF2 α phosphorylation, one of the pathways that also activates TFEB; iii) TFEB activation promotes ATF4 expression [28]; iv) TFEB activation via cellular stress response may be sustained longer at a low level for as long as the stimuli persists, while the activation via upstream kinase inhibition is usually limited to a few hours; v) upstream kinase inhibition may compromise normal immune response during infection; vi) luminescence read-outs provide easy detection with excellent signal-to-noise ratio and can be easily developed into an HTS format.

The temporal and spatial activation of TFEB inside the cells by small molecules could be very heterogeneous, therefore putting limitations on current screening approaches that follow TFEB nuclear translocation as

a readout and restricting hit selection to compounds that activate TFEB within a single timepoint and register a strong response. This leads to the identification of compounds with pleiotropic activities and immediate inhibition of kinases, channels, or other protein targets upstream of TFEB. We reasoned that casting a wider net on the small molecules where response is measured within a longer timeframe and with a more robust signal could enable identification of potential TFEB activators that act more slowly or in a more sustained manner. The ATF4 luciferase reporter cell line we developed offered a robust signal-to-noise ratio with a Nano-Glo luciferase biochemical assay (Promega), good reproducibility and ease of execution in an HTS format. We selected a 24 h timepoint to ensure that hits would include compounds that activate TFEB early with subsequent ATF4 induction in a TFEB-dependent manner, as well as the compounds that activate ATF4 first and promote TFEB activation later. The later timepoint also allowed for greater accumulation of the reporter to include compounds that may produce milder integrated stress response or activate TFEB to a lesser degree.

We identified 21 compounds that activated the integrated stress response via ATF4 and induced ATF4-dependent reporter expression. Of those compounds, at least two classes of identified compounds, proteasome inhibitors and anti-malarial artemisinin and its endoperoxide derivatives, consistently and potently activated TFEB. Another hit, resveratrol, a pleiotropic agent with many biological activities, was reported to activate TFEB [27]. The antimalarial hit artesunate has also been shown to induce ER stress and increase expression of ATF4 and CHOP in cancer cells at concentrations of 5 μ M and above [29]. Our results are consistent with previous reports and demonstrate significant luminescence even at nanomolar concentrations after 24 hours of exposure, suggesting that TFEB activation is likely to be observed at lower concentrations as well.

It is likely that out of the identified hits many other compounds activate TFEB but the response kinetics, and potency could differ vastly among different agents and should be studied individually. We limited our reporter luminescence measurements to a 24-h timepoint to minimise the possibility of false negatives that result from cytotoxicity when screening thousands of compounds. Both thapsigargin and tunicamycin produced a significant luminescent signal by this time point in the assay at concentrations similar to those used during screening.

Proteasome inhibitors were identified among the most potent activators of TFEB and autophagy in response to stress. This is consistent with proteasome inhibitors exerting proteotoxic stress via accumulation of misfolded proteins and ER stress. This observation led us to hypothesise and test if the Mtb selective proteasome inhibitors may act with dual activities via targeting Mtb proteasome directly as well as promoting host TFEB activation to improve lysosomal function. Two different Mtb-active proteasome inhibitors with variable selectivity against human proteasomes activated TFEB in BMDM

within 2 h of exposure depending on the degree of their selectivity for the Mtb versus the human proteasome, suggesting that less selective Mtb proteasome inhibitors could provide the benefit of dual activities targeting Mtb directly as well as promoting host activities to aid clearance. This dual activity of Mtb proteasome inhibitors echoes another TB drug, bedaquiline, reported to activate host TFEB albeit by a different mechanism [15].

Our data add to previous studies focused on the identification of small molecule TFEB activators by offering a different approach, which is easy, robust, reproducible and works in an HTS format. The assay can potentially identify fast and slow acting TFEB activators which consequently will lead to ATF4 induction as well as compounds that act primarily to activate the integrated stress response and ATF4 and then promote TFEB activation in response to stress. We test screened a small library of FDA-approved drugs and other research compounds to validate the assay and demonstrate that we were able to identify compounds in several clinical uses, including antibiotics, anti-parasitics, and anti-cancer drugs as potential ATF4 and TFEB activating compounds.

A greater appreciation of host-specific effects may allow for better rationalisation of future anti-infective development efforts. For example, the mycobacterial ATP synthase inhibitor bedaquiline has recently been shown to exert host cell-specific effects [15]. Drugs that exert both host specific and direct, bactericidal actions may be the more efficacious in reducing bacterial burdens and improving outcomes. In summary, we describe the development and methods for an ATF4-reporter luciferase HTS assay to identify compounds that activate ATF4 and TFEB transcription factors in host cells. These results justify an expanded search as well as future testing in models of infection.

Methods

Cell lines and bone marrow derived macrophages

HEK293T and Raw 264.7 cells were cultured in DMEM supplemented with 10% FBS, 1% HEPES, 1% sodium pyruvate, and 1% L-glutamine (cDMEM). Bone marrow-derived macrophages (BMDM) were isolated from femurs of female C57BL6 mice and differentiated for 1 week in DMEM supplemented with 10% FBS, 1% HEPES, 1% sodium pyruvate, 1% L-glutamine and 20% L929 cell conditioned media (LCM). All cells were grown at 37 degrees C, 5% CO₂. After 1 week, cells were lifted with 1 mM EDTA in PBS, collected, and plated in DMEM supplemented with 10% FBS, 1% HEPES, 1% sodium pyruvate, 1% L-glutamine, and 10% LCM. Hank's Balanced Salt Solution (HBSS, Gibco catalogue number 14175103) was used where indicated. No antibiotics were used during BMDM differentiation or BMDM and RAW treatment with test compounds.

pNL(NlucP/ATF4-RE/Hygro) vector preparation

The pNL(NlucP/ATF4-RE/Hygro) vector was purchased from Promega. DNA was transformed into Mach1 *E. coli* and streaked on LB agar plates supplemented with ampicillin or carbenicillin. Selected colonies were grown in 2 mL of 2YT broth for at least 3 hours at 37 degrees C. 20 μ L of culture was then used to inoculate 20 mL of 2YT broth and incubated overnight at 37 degrees C. Bacteria were pelleted and DNA isolated into three separate aliquots using the QIAprep Spin Miniprep kit (Qiagen 27106) as per the manufacturer's instructions. DNA was quantified using a NanoDrop One (Thermo Scientific).

pNLUC-ATF4 transfection optimisation in HEK293T cells and selection in hygromycin

HEK293T cells were cultured in cDMEM and plated in six well plates at a density of 5×10^5 cells/well, allowed to grow overnight and then transfected using either Lipofectamine LTX or Lipofectamine 3000 using the parameters outlined in Supplemental Table 1 and according to the manufacturer's instructions. Transfections were stopped at the indicated time points, and cells from all conditions were then plated in 96 well plates (Corning 3903) and treated with either thapsigargin (1 μ M) or compound 2062 (3 μ M). Cells were incubated for 6.5 to 7.5 hours and luminescence measured using the Nano-Glo Luciferase Assay System (N1130) from Promega as per the manufacturer's instructions. Signal was detected on a SpectraMax iD5 microplate reader (Molecular Devices) and data expressed as either RLUs or % change vs control. For stable transfection, HEK293T cells were plated at a density of 5×10^5 cells per well in a six well plate, allowed to grow overnight and transfected the following morning. Cells were transfected using Lipofectamine LTX, 15 μ L of transfection reagent and 1 μ g plasmid DNA for 66.5 hours. After 66.5 hours, both transfected and non-transfected control cells were washed and passaged to 8×10^4 cells/well in six well plates in media containing either 150 μ g/mL or 300 μ g/mL hygromycin B. A subset of cells was treated with thapsigargin immediately after transfection to measure the luminescent signal (Supplemental Figure 2). Media was replaced every 2–3 days, and cells were monitored for viability. After 17 days, all non-transfected cells had died and transfected cells exposed to both concentrations of hygromycin were passaged for further selection and testing. A subset of cells was plated at a density of 5×10^4 cells/well in 96 well plates in media that either included or excluded hygromycin at the concentration used for selection of that cell population. These conditions were kept consistent during treatment with thapsigargin for testing. Luminescence was measured using the NanoGlo Luciferase Assay System (N1130) from Promega as per the manufacturer's instructions. Signal was detected on a SpectraMax iD5

microplate reader (Molecular Devices). Results are expressed as % change vs control cells and calculated as follow: ((raw data sample-negative control mean)/negative control mean)*100.

Luciferase assays of Tunicamycin and Thapsigargin dose responses over time

Dilutions of tunicamycin or thapsigargin were prepared in cell culture media and plated in 384 well plates (Corning 3765) at concentrations 2x to indicated final dilutions in 25 μ L per well. For the tunicamycin time course, cells were then plated on top of these dilutions at a concentration of 3×10^4 cells/25 μ L/well and incubated for the indicated times. For the thapsigargin time course, cells were plated at the Rockefeller University Fisher DDRC using a Thermo MultiDrop liquid handling machine at a density of 2.5×10^4 cells/25 μ L/well and incubated for the indicated times. Luminescence was measured using the Nano-Glo Luciferase Assay System (N1130) from Promega as per the manufacturer's instructions by adding 50 μ L prepared luciferase assay reagent to each well. For the tunicamycin time course, signal was detected on a SpectraMax iD5 microplate reader (Molecular Devices). For the thapsigargin time course, signal was detected on a BioTek Synergy Neo microplate reader at the Rockefeller University Fisher DDRC. Results are expressed as % change vs untreated control and calculated as follows: ((raw data sample-negative control mean)/negative control mean)*100.

Cell density optimisation, LOPAC library, and modified Selleck Chemicals library luciferase assays

Cell density optimisation and all screening were performed at the Rockefeller University Fisher DDRC. For cell density optimisation, thapsigargin was prepared in cell culture media at 2 μ M and plated in 384 well plates (Corning 3765) in 25 μ L per well. Cells were then plated on top of these dilutions using a Thermo MultiDrop liquid handling machine at the Rockefeller University Fisher DDRC at the cell densities indicated and incubated for 24 hours. Luminescence was measured using the Nano-Glo Luciferase Assay System (N1130) from Promega as per the manufacturer's instructions by adding 50 μ L prepared luciferase assay reagent to each well using the Thermo MultiDrop liquid handling machine at the Rockefeller University Fisher DDRC. Signal was detected on a BioTek SynergyNeo microplate reader. Results are expressed in relative luminescent units (RLUs). For screening the LOPAC library, library compounds were diluted in cell culture media and dispensed into 384 well plates (Corning 3765) at concentrations 2x to indicated final dilutions in 25 μ L per well. All plates included negative control DMSO wells and 1 μ M thapsigargin positive control wells. Cells were then plated on top of these dilutions

using a Thermo MultiDrop liquid handling machine at the Rockefeller University Fisher DDRC at a concentration of 3×10^4 cells/25 μ L/well and incubated for 24 hours. Luminescence was measured using the Nano-Glo Luciferase Assay System (N1130) from Promega as per the manufacturer's instructions by adding 50 μ L prepared luciferase assay reagent to each well using the Thermo MultiDrop liquid handling machine at the Rockefeller University Fisher DDRC. Signal was detected on a BioTek Synergy Neo microplate reader. Results are expressed as percent activation and were calculated as follows: $((\text{raw data sample value} - \text{negative control mean}) / (\text{positive control mean} - \text{negative control mean})) \times 100$. The screen of the modified Selleck Chemicals library was performed exactly as the LOPAC library.

Dose response evaluation of library screen hits luciferase assay

Eleven two-fold dilutions starting at a maximum of 8 μ M concentration were prepared in cell culture media for the top 48 hit compounds and plated in 384 well plates (Corning 3765) at the Rockefeller University Fisher DDRC. Cells were then plated on top of these dilutions using a Thermo MultiDrop liquid handling machine at the Rockefeller University Fisher DDRC at a concentration of 3×10^4 cells/25 μ L/well and incubated for 24 hours. Luminescence was measured using the Nano-Glo Luciferase Assay System (N1130) from Promega as per the manufacturer's instructions by adding 50 μ L prepared luciferase assay reagent to each well using the Thermo MultiDrop liquid handling machine at the Rockefeller University Fisher DDRC. Signal was detected on a Biotek Synergy Neo microplate reader. Results are expressed as % DMSO controls. EC₅₀ values were calculated using the Collaborative Drug Discovery website.

Modified Selleck Chemicals library

The library consists of approximately 1800 clinical drug samples selected from Selleck Chemicals Inc.'s database of known drugs and clinical research compounds. Most compounds from this database have been removed, including all topical compounds; compounds legal only in India, China, Russia, or other less rigorous jurisdictions; compounds only patented or published with no jurisdictional approval; compounds that have been grandfathered in due to common use prior to the modern era of the FDA; nutraceuticals; and compounds with extreme molecular weight, cLogP, or Polar Surface Area or replicate structures with various formulations. The remaining drugs are legally marketed in the USA and/or Great Britain, the European Union and/or Japan or undergoing legally approved clinical trials in at least one of these jurisdictions with good medicinal chemical properties.

Chemical compounds

Chemical compounds tested in the screen were provided by the Rockefeller Fisher DDRC. All secondary test compounds used in cell culture and for follow-up assays are commercially available and were purchased as follows: Hygromycin B (400052) from EMD Millipore. Bortezomib (10008822), carfilzomib (17554), thapsigargin (10522), torin1 (10,997), Ikarugamycin (15386) were from Cayman Chemical Company. Tunicamycin (T7765), ethambutol (E4630), isoniazid (I3377), and rifampin (R3501) were from Sigma. Bedaquiline (A12327), and ouabain (A12755) were from AdooQ. Compound 2062 was provided by Celgene (BMS).

Antibodies

TFEB (Bethyl Laboratories, Inc., A303673a). ATF4 (Cell Signalling technologies, 11815). B Actin (Santa Cruz Biotechnology, sc-47778). P62 (Sigma, P0067). LC3 (Sigma, L8918).

Western blots

Raw 264.7 cells were seeded at $2-5 \times 10^6$ cells/well in a six well plate in 2 ml of cDMEM. Treatment with tunicamycin or exposure to HBSS starvation was carried out for 7 hours, cells washed three times with PBS and cells lysed RIPA buffer supplemented with 1 mM PMSF and the protease inhibitor tablet (Roche). For ATF4 and actin staining, 40 μ g of protein was loaded into 10% SDS PAGE gels.

For [Figures 5 and 7](#), mouse bone marrow-derived macrophages (BMDMs) were isolated and cultured as described above. BMDMs were seeded at a density of 2×10^6 cells/well in six well plates and treated with the indicated concentrations of compounds. Separation of nuclear and cytoplasmic proteins was accomplished using NE-PER cytosolic and nuclear separation kit (Thermo #78833) as per the manufacturer's instructions. Cytoplasmic extraction and nuclear extraction buffers were supplemented with 1 mM PMSF and the protease inhibitor tablet (Roche). For [Figure 8](#), soluble cellular extracts were prepared in a RIPA buffer supplemented with 1 mM PMSF and the protease inhibitor tablet (Roche) and separated on a 15% SDS-PAGE. Secondary antibodies were IRDye 680 and 800 (Licor). Images were acquired on an Azure Biosystems c600 imaging system. WB were analysed by Fiji (ImageJ) and normalised to the levels of loading controls (actin for the cytosolic proteins and histone H3 for the nuclear proteins) in each lane. For each WB panel, a protein band signal in control lanes (NC, vehicle control) was designated as "1" and the signal levels in treated samples were

calculated relative to NC after normalisation to loading control. Statistical analysis was performed by one-way ANOVA and multiple comparisons were carried out for the treated vs control samples in GraphPad Prism 10 with a P value calculation at a confidence level of 95% (definition of statistical significance between the samples: $P < 0.05$). Adjusted P values for multiple comparisons by the Dunnett's test are displayed under the brackets in each figure.

Immunocytochemistry and confocal microscopy

BMDM were seeded 1×10^5 cells/well in 0.5 mL media supplemented with 10% L929 cell conditioned media. Cells were allowed to adhere overnight, and the following morning media was aspirated and replaced with the specified compounds at the indicated doses and times. Cells were then washed once with PBS and fixed with 4% PFA in PBS for 15 minutes at room temperature. Cells were washed three times with PBS, permeabilized with 0.2% TriX100 in PBS for 10 minutes at room temperature, washed again three times with 0.1% TriX100 in PBS and then incubated in 2% BSA-0.1% TriX100-0.1% NaN_3 in PBS for 1 h at room temperature. After blocking, cells were incubated with anti-TFEB (A303673a, Bethyl Laboratories, Inc.) diluted 1:100 in 2% BSA-0.1% TriX100-0.1% NaN_3 in PBS at 4 degrees C overnight. The next day, cells were washed with 0.1% TriX100 in PBS five times and incubated with the secondary goat anti-rabbit IgG (H + L) Alexa Fluor Plus 647 (Invitrogen) antibody at 1:200 in 2% BSA-0.1% TriX100-0.1% NaN_3 in PBS for 1 h at room temperature. Cells were again washed three times in 0.1% TriX100 in PBS and then DNA stained with Hoechst 33342 DNA dye (Molecular Probes) diluted in PBS for 10 minutes at room temperature. Cells were washed once with 0.1% TriX100 in PBS and slides mounted. Images were taken using a Zeiss 880 laser scanning confocal microscope with an oil immersion lens at 40x. Images were processed in ImageJ using a macro function provided by the Weill Cornell microscopy and imaging core that outlined the perimeter of individual nuclei and then measured red, mean fluorescence intensity within the identified boundaries of DNA staining of all nuclei within a given image. Partial nuclei on image borders were excluded from the analysis.

Statistics

Comparisons for immunocytochemistry experiments between multiple groups were performed in Prism using one-way ANOVA with post hoc Dunnett's test. Statistical analysis for ImageJ WB densitometry was done by one-way ANOVA, and multiple comparisons were carried out for the treated

vs control samples in GraphPad Prism 10 with a P value calculation at a confidence level of 95% (definition of statistical significance between the samples: $P < 0.05$). Adjusted P values for multiple comparisons were obtained by the Dunnett's test.

Acknowledgments

We are grateful to Prof. Carl Nathan for his support (NIH R01AI138940) and discussions. This work was supported by the Abby and Howard P. Milstein Program in Chemical Biology and Translational Medicine at WCM. The Department of Microbiology and Immunology is supported by the William Randolph Hearst Trust. We thank the the Rockefeller University Fisher DDRC's (resource center ID RRID:SCR_020985) Victor Bustos, PhD, J. Fraser Glickman, PhD, and Chloe Larson for assistance, advice and support; WCM's Microscopy and Imaging Core Facility Lee Cohen-Gould, MS, CEMT, Sushmita Mukherjee, PhD, and Janet Sun for assistance and support. Carfilzomib, bortezomib, and Mtb proteasome inhibitors 6 and 11 were provided by Gang Lin, PhD.

Abbreviation

ATF4, activating transcription factor 4; BMDM, bone marrow derived macrophages; cDMEM, complete Dulbecco's Modified Eagle Medium; EC_{50} , half maximal effective concentration; ER, endoplasmic reticulum; FDA, U.S. Food and Drug Administration; HDT, host-directed therapy; HEK293T, human embryonic kidney 293 cell line expressing the simian virus 40 large T antigen; HTS, high throughput screening; Mtb, *Mycobacterium tuberculosis*; mTOR, mammalian target of rapamycin kinase; TB, tuberculosis; TFEB, transcription factor E-box.

Disclosure statement

No potential conflict of interest was reported by the author(s).

Funding

This work was supported by the NIH R01AI138940 (PI, Nathan) and by the Abby and Howard P. Milstein Program in Chemical Biology and Translational Medicine at WCM. The Department of Microbiology and Immunology is supported by the William Randolph Hearst Trust.

ORCID

Ruslana Bryk  <http://orcid.org/0000-0002-2179-671X>

References

- [1] Tobin DM. Host-directed therapies for tuberculosis. *Cold Spring Harb Perspect Med.* **2015**;5(10):a021196.
- [2] Young C, Walzl G, Du Plessis N. Therapeutic host-directed strategies to improve outcome in tuberculosis. *Mucosal Immunol.* **2020**;13(2):190–204.
- [3] Wallis RS, Ginindza S, Beattie T, et al. Adjunctive host-directed therapies for pulmonary tuberculosis: a prospective, open-label, phase 2, randomised controlled trial. *Lancet Respir Med.* **2021**;9(8):897–908.
- [4] Zheng W, Chang IC, Limberis J, et al. Mycobacterium tuberculosis resides in lysosome-poor monocyte-derived lung cells during chronic infection. *PLoS Pathog.* **2024**;20(5):e1012205. doi:[10.1371/journal.ppat.1012205](https://doi.org/10.1371/journal.ppat.1012205)
- [5] Goldberg MF, Saini NK, Porcelli SA. Evasion of innate and adaptive immunity by Mycobacterium tuberculosis. *Microbiol Spectr.* **2014**;2(5). doi:[10.1128/microbiol.spec.MGM2-0005-2013](https://doi.org/10.1128/microbiol.spec.MGM2-0005-2013)
- [6] Queval CJ, Song O-R, Carralet J-P, et al. Mycobacterium tuberculosis controls phagosomal acidification by targeting CISH-mediated signaling. *Cell Rep.* **2017**;20(13):3188–3198.
- [7] Clemens DL, Horwitz MA. Characterization of the Mycobacterium tuberculosis phagosome and evidence that phagosomal maturation is inhibited. *J Exp Med.* **1995**;181(1):257–270.
- [8] Clemens DL, Lee BY, Horwitz MA. Mycobacterium tuberculosis and Legionella pneumophila phagosomes exhibit arrested maturation despite acquisition of Rab7. *Infect Immun.* **2000**;68(9):5154–5166.
- [9] Malik ZA, Denning GM, Kusner DJ. Inhibition of Ca(2+) signaling by Mycobacterium tuberculosis is associated with reduced phagosome-lysosome fusion and increased survival within human macrophages. *J Exp Med.* **2000**;191(2):287–302.
- [10] Cooper AM, Mayer-Barber KD, Sher A. Role of innate cytokines in mycobacterial infection. *Mucosal Immunol.* **2011**;4(3):252–260.
- [11] Sousa J, Cá B, Maceiras AR, et al. Mycobacterium tuberculosis associated with severe tuberculosis evades cytosolic surveillance systems and modulates IL-1 β production. *Nat Commun.* **2020**;11(1):1949.
- [12] Ouimet M, Koster S, Sakowski E, et al. Mycobacterium tuberculosis induces the miR-33 locus to reprogram autophagy and host lipid metabolism. *Nat Immunol.* **2016**;17(6):677–686.
- [13] Fu Y, Yi Z, Wu X, et al. Circulating microRNAs in patients with active pulmonary tuberculosis. *J Clin Microbiol.* **2011**;49(12):4246–4251.
- [14] Bryk R, Mundhra S, Jiang X, et al. Potentiation of rifampin activity in a mouse model of tuberculosis by activation of host transcription factor EB. *PLOS Pathog.* **2020**;16(6):e1008567.
- [15] Giraud-Gatineau A, Coya JM, Maure A, et al. The antibiotic bedaquiline activates host macrophage innate immune resistance to bacterial infection. *Elife.* **2020**;9. doi:[10.7554/eLife.55692](https://doi.org/10.7554/eLife.55692).
- [16] Schuster EM, Epple MW, Glaser KM, et al. TFEB induces mitochondrial itaconate synthesis to suppress bacterial growth in macrophages. *Nat Metab.* **2022**;4(7):856–866.
- [17] Settembre C, Di Malta C, Polito VA, et al. TFEB links autophagy to lysosomal biogenesis. *Science.* **2011**;332(6036):1429–1433.

- [18] Roczniak-Ferguson A, Petit CS, Froehlich F, et al. The transcription factor TFEB links mTORC1 signaling to transcriptional control of lysosome homeostasis. *Sci Signal.* **2012**;5(228):ra42.
- [19] Medina DL, Di Paola S, Peluso I, et al. Lysosomal calcium signalling regulates autophagy through calcineurin and TFEB. *Nat Cell Biol.* **2015**;17(3):288–299.
- [20] Tong Y, Song F. Intracellular calcium signaling regulates autophagy via calcineurin-mediated TFEB dephosphorylation. *Autophagy.* **2015**;11(7):1192–1195.
- [21] Napolitano G, Esposito A, Choi H, et al. mTOR-dependent phosphorylation controls TFEB nuclear export. *Nat Commun.* **2018**;9(1):3312.
- [22] Wang C, Niederstrasser H, Douglas PM, et al. Small-molecule TFEB pathway agonists that ameliorate metabolic syndrome in mice and extend *C. elegans* lifespan. *Nat Commun.* **2017**;8(1):2270.
- [23] Chao X, Niu M, Wang S, et al. High-throughput screening of novel TFEB agonists in protecting against acetaminophen-induced liver injury in mice. *Acta Pharm Sin B.* **2024**;14(1):190–206.
- [24] Carling PJ, Ryan BJ, McGuinness W, et al. Multiparameter phenotypic screening for endogenous TFEB and TFE3 translocation identifies novel chemical series modulating lysosome function. *Autophagy.* **2023**;19(2):692–705.
- [25] Song JX, Sun Y-R, Peluso I, et al. A novel curcumin analog binds to and activates TFEB in vitro and in vivo independent of MTOR inhibition. *Autophagy.* **2016**;12(8):1372–1389.
- [26] Yang C, Su C, Iyaswamy A, et al. Celastrol enhances transcription factor EB (TFEB)-mediated autophagy and mitigates Tau pathology: implications for Alzheimer's disease therapy. *Acta Pharm Sin B.* **2022**;12(4):1707–1722.
- [27] Shao R, Shi J, Du K, et al. Resveratrol promotes lysosomal function via ER calcium-dependent TFEB activation to ameliorate lipid accumulation. *Biochem J.* **2021**;478(5):1159–1173.
- [28] Martina JA, Diab HI, Brady OA, et al. TFEB and TFE 3 are novel components of the integrated stress response. *EMBO J.* **2016**;35(5):479–495.
- [29] Wang N, Zeng G-Z, Yin J-L, et al. Artesunate activates the ATF4-CHOP-CHAC1 pathway and affects ferroptosis in Burkitt's Lymphoma. *Biochem Biophys Res Commun.* **2019**;519(3):533–539.
- [30] Lin G, Li D, de Carvalho LPS, et al. Inhibitors selective for mycobacterial versus human proteasomes. *Nature.* **2009**;461(7264):621–626.
- [31] Zhang H, Hsu H-C, Kahne SC, et al. Macrocyclic peptides that selectively inhibit the *Mycobacterium tuberculosis* Proteasome. *J Med Chem.* **2021**;64(9):6262–6272.
- [32] Sha Z, Schnell HM, Ruoff K, et al. Rapid induction of p62 and GABARAPL1 upon proteasome inhibition promotes survival before autophagy activation. *J Cell Biol.* **2018**;217(5):1757–1776.
- [33] Pan B, Li J, Parajuli N, et al. The calcineurin-TFEB-p62 pathway mediates the activation of cardiac macroautophagy by proteasomal malfunction. *Circ Res.* **2020**;127(4):502–518.
- [34] Klionsky DJ, Abdel-Aziz AK, Abdelfatah S, et al. Guidelines for the use and interpretation of assays for monitoring autophagy (4th edition). *Autophagy.* **2021**;17(1):1–382.
- [35] Chandra P, Grigsby SJ, Philips JA. Immune evasion and provocation by *Mycobacterium tuberculosis*. *Nat Rev Microbiol.* **2022**;20(12):750–766.